Applied Thermal Engineering 72 (2014) 90–96

Contents lists available at ScienceDirect

Applied Thermal Engineering

journal homepage: www.elsevier.com/locate/apthermeng

Shape optimization of inlet part of a printed circuit heat exchanger using surrogate modeling

Gyoung-Wan Koo, Sang-Moon Lee, Kwang-Yong Kim*

Department of Mechanical Engineering, Inha University, Incheon 402-751, Republic of Korea

HIGHLIGHTS

- Shape optimization of inlet part of a PCHE was performed using 3-D RANS analysis and surrogate modeling.
- Objective function is weighted sum of the objectives related to flow uniformity (F_f) and pressure drop (F_P).
- Objective function was reduced by 1.36 and 1.18%, respectively, by the RBNN and KRG compared to reference.
- F_f was increased by 7.5% while F_P was decreased by 7.6% by KRG compared to reference.
- Errors between objective function values predicted by surrogates and RANS analysis were only about 3.0%.

ARTICLE INFO

Article history:
Received 30 August 2013
Accepted 5 December 2013
Available online 14 December 2013

Keywords:
Printed circuit heat exchanger
Inlet plenum
Shape optimization
RANS analysis
Flow uniformity
KRG
RBNN

ABSTRACT

Aim of the present work is to optimize the shape of inlet part of a printed circuit heat exchanger to enhance the thermal–hydraulic performance using surrogate modeling. The fluid flow was analyzed using three-dimensional Reynolds-averaged Navier–Stokes analysis with the shear stress transport turbulence model. The non-dimensional parameters related to the angle and radius of curvature of the inlet plenum wall, and diameter of the inlet pipes were selected as design variables for the optimization. The objective function was defined as a weighted-sum of two objectives related to uniformity of the mass flow rate distribution and pressure loss, respectively. Twenty six design points were obtained by Latin hypercube sampling method. The Kriging and the radial basis neural networks were used as surrogate models to approximate the value of the objective function. The results of the optimization with a weighting factor show that the objective function values of the optimum designs obtained by the two surrogate models were similar to each other and improved from that of the reference design.

1. Introduction

Recently, the gas turbine cycle, which has the advantages such as simplicity and efficiency in comparison with the steam turbine cycle, has been considered as a potential nuclear power generation for the future. However, the harsh environment of gas turbine cycle, such as high temperature and pressure, may cause the instability of the system operation. Furthermore, the inefficiency due to the large volume is inevitable since gas is used as a working fluid. Printed circuit heat exchanger (PCHE), which is suitable for the gas turbine cycle due to high pressure resistance and compactness, was developed by HEATRIC [1] in order to overcome these operating conditions. Actually, PCHEs are smaller and lighter than cell & tube type heat exchangers which have similar performance. On the other hand, PCHEs are made through chemical etching and diffusion bonding. Therefore, operation of PCHEs is more stable and effective than the other types of heat exchanger. Fig. 1 [2] shows the outline of the inlet part of the PCHE. As shown in this figure, the main stream is distributed to branch channels through the inlet plenum.

During the last decade, many research works have been performed on PCHEs both experimentally and numerically. Mostly these studies were performed for geometry construction with zigzag channels and proper operating conditions of PCHE. Ishizuka et al. [3] analyzed the characteristics of a PCHE in terms of the thermal performance and pressure drop of supercritical carbon-dioxide (CO_2) in the PCHE under variations of the flow rate, pressure, and temperature. Ngo et al. [4] performed numerical analysis to compare the performance of a PCHE channel with an S-shaped fin with that of a reference PCHE channel using three-dimensional Reynolds-averaged Navier–Stokes (3-D RANS) analysis. Nikitin

* Corresponding author. Department of Mechanical Engineering, Inha University, 253 Yonghyun-Dong, Nam-Gu, Incheon 402-751, Republic of Korea. Tel.: +82 32 872 3096; fax: +82 32 868 1716.
E-mail address: kykim@inha.ac.kr (K.-Y. Kim).

1359-4311/$ – see front matter © 2013 Elsevier Ltd. All rights reserved.
http://dx.doi.org/10.1016/j.applthermaleng.2013.12.009

et al. [5] obtained the thermal–hydraulic characteristics of a PCHE in an experiment with a supercritical carbon-dioxide loop. Kim et al. [6] performed a comparative study on zigzag and airfoil-shaped fin PCHEs using 3-D numerical analysis. They showed that the airfoil-shaped fin PCHE had almost the same total heat transfer rate per unit volume and decreased pressure drop compared with the zigzag PCHE. Kim et al. [7] performed a numerical study on the flow characteristics and thermal performances of PCHEs using RANS analysis. Lee et al. [8] performed a multi-objective optimization to enhance the heat transfer performance and to reduce the pressure drop in zigzag channels of a PCHE with three geometrical parameters. Many researches have been performed on the flow and heat transfer in the channels of PCHEs, but only focused on the zigzag part of the PCHE channels. However, the inlet plenum of the PCHE is also important, because high pressure loss and non-uniformity in the mass flow distribution may occur in this inlet region.

On the other hands, the optimization technique combined with RANS analysis has been widely adopted in the field of engineering application. Kim and Kim [9] performed optimization of a vane diffuser in a mixed-flow pump to improve the efficiency using optimization technique. And, they obtained the result that the efficiency at the design flow coefficient was improved by 7.05% and the off-design efficiencies were also improved in comparison with the reference design. Kim and Kim [10] obtained the optimum shape of 3-D channel roughened by angled ribs using optimization technique with RANS analysis. They reported that optimal values of rib pitch-to-rib height ratio and rib displacement-to-rib height ratio increase, but those of attack angle and rib height-to-channel height ratio decrease as design emphasis was shifted to reduction of friction loss. Husain and Kim [11] performed an optimization of a rectangular micro-channel heat sink for minimum thermal resistance using surrogate models. They founded that thermal resistance of the heat sink was more sensitive to channel width-to-depth ratio than fin width-to-depth ratio around the optimal point. Raza and Kim [12] carried out a shape optimization of a wire-wrapped fuel assembly using Kriging meta-modeling technique. They defined the objective function as a linear combination of heat transfer and friction loss related terms with a weighing factor.

Recently, Lee et al. [13] performed a parametric study on inlet part of a PCHE, where the effects of geometric variables on hydraulic performance of the PCHE have been tested numerically. In the present work, the inlet part of the PCHE was optimized using surrogate-based optimization techniques with three non-dimensional design variables related to the angle and radius of curvature of the inlet plenum wall, and diameter of the inlet pipes, respectively. For the optimization, numerical analysis was performed in the inlet part of the PCHE using 3-D RANS. The Kriging (KRG) [14] and radial basis neural networks (RBNN) [15] models were used as the surrogate models to approximate the objective functions for the optimization. Twenty-six experimental points in design space were chosen by Latin Hypercube Sampling (LHS) [16] for the three design variables.

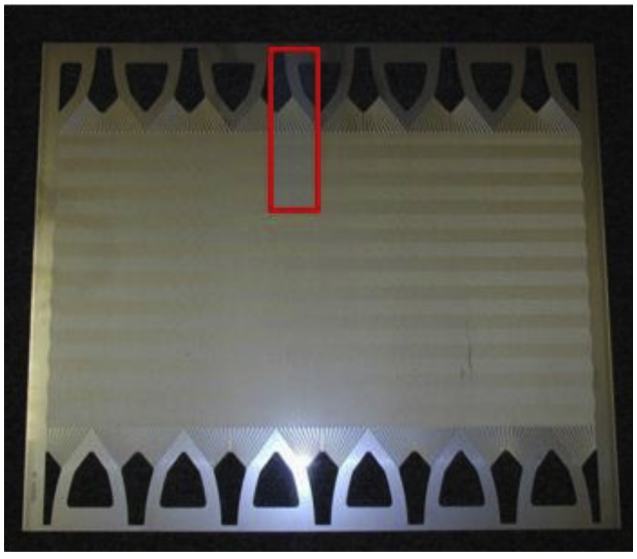

Fig. 1. Example of full size platelet [2].

2. Numerical analysis

3-D RANS analyses of the fluid flow and convective heat transfer were conducted by using ANSYS-CFX 11.0 [17]. The solutions were obtained by solving the compressible RANS equations through the finite-volume method to discretize the governing differential equations in the inlet part of PCHE. Shear stress transport (SST) model [18] was employed as turbulence closure. SST model combines the advantages of the k–ε and k–ω models with a blending function. The k–ω is activated in the near-wall region, and the k–ε is used in the region far from the wall. Bardina et al. [19] reported that the SST model efficiently captures separation under an adverse pressure gradient compared to the other eddy viscosity models.

Fig. 2 shows the reference geometry of the inlet part of PCHE constructed based on the experimental work of Ishizuka et al. [3]. This inlet part consists of three sub-parts, namely, zigzag channels, inlet pipes, and inlet plenum. And, the dimensions of reference geometry of PCHE are given in Table 1. The boundary conditions and physical properties, which were used for numerical analysis of inlet part of PCHE, are listed in Table 2 based on the experimental work of Ishizuka et al. [3]. An example of grid system in the calculation domain is shown in Fig. 3. To construct the volume meshes, unstructured tetrahedral meshes were employed in most of the domain, and the prism meshes were used near the walls. High resolution scheme was selected for discretizing the governing equations.

A turbulence intensity of 5% and an auto-computed length scale were selected for the inlet turbulence conditions. The first grid points adjacent to the walls are placed at $y+$ less than 1.0, which is required to implement the low-Reynolds-number SST model. A residual reduction factor of 10^{-6} was used for the convergence of the iterative solutions. A personal computer with an Intel core I7 2.4 GHz CPU was used for the computations, and the total time for getting each converged solution was in the range of 20–23 h.

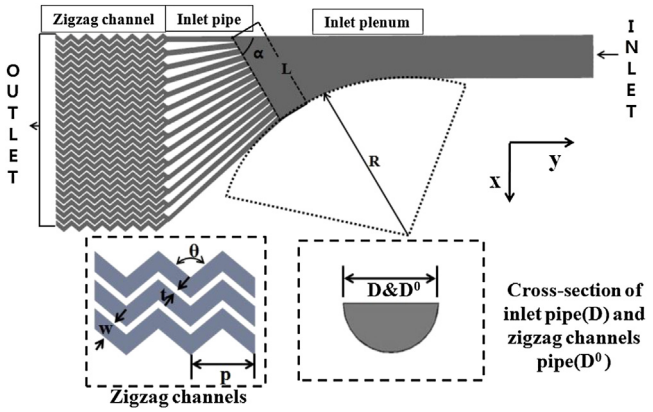

Fig. 2. Geometry of the inlet part in the PCHE.

Table 1
Dimensions of reference geometry of the PCHE.

Parameters of reference geometry	Value
Angle of zigzag channels, θ	100°
Wall thickness of zigzag channels, t	0.60 mm
Pitch length of zigzag channels, p	7.24 mm
Width of zigzag channels, w	1.90 mm
Angle of the inlet plenum wall, α	60°
Radius of curvature of the inlet plenum wall, R	84.4 mm
Width of the inlet plenum wall connected to inlet pipes, L	45.86 mm
Diameter of zigzag channel, D^0	1.80 mm
Diameter of inlet pipe, D	2.70 mm

3. Optimization procedure

Fig. 4 is the flow chart which shows the optimization procedure using surrogate modeling. In the first step, the objective function and design variables are chosen for the optimization procedure. The design space is then decided from a parametric study [13] for improved system performance. Experimental points are selected through the design of experiments. At these experimental points, the objective function values are calculated using RANS analysis. Finally, the surrogate model is constructed, and then optimal point is searched by the optimal point search algorithm.

3.1. Design variables and objective function

Design variables for optimization were decided based on the results obtained by the parametric study [13]. Three non-dimensional variables, i.e., the angle of the inlet plenum wall (α), ratio of the radius of curvature to the width of inlet plenum (R/L), and ratio of diameter of inlet pipes to diameter of zigzag channels (D/D^0), were used as design variables for the optimization.

The objective function was defined as a weighted-sum of two objectives related to uniformity of the mass flow rate distribution and pressure loss, respectively. The uniformity of mass flow rates distributed to the zigzag channels was calculated by standard deviation of the non-dimensional mass flow parameter, S_i defined as follow:

$$F_f = \sqrt{\mathrm{Var}[S_i]} \tag{1}$$

$$S_i = \frac{m_i}{m_{avg}} \tag{2}$$

where, m_i is mass flow rate in i_{th} zigzag channel, and m_{avg} is mass flow rate averaged over the zigzag channels.

The non-dimensional pressure drop related to the pressure drop in the inlet plenum of the PCHE was defined as

$$F_p = \frac{p_{in} - p_{out}}{0.5\rho v^2} \tag{3}$$

where, p_{in} and p_{out} are total pressures at inlet and outlet of inlet plenum, respectively. ρ indicates fluid density of supercritical CO_2. v indicates the average velocity in the inlet plenum of the PCHE.

Finally, the objective function was defined using a weighted-sum of the above two objectives as follow:

$$F = F_f + \beta F_P \tag{4}$$

Thus, the present optimization problem is to minimize the objective function, F with the weighting factor, β, which is selected as per design requirement.

3.2. Design of the experiment

In order to construct the surrogate model for the objective function, some design points are required for filling the design space. These can be established through an experimental design. LHS [16] is an effective sampling method that uses an $m \times n$ simulation matrix, where m is the number of sampling points to be examined and n is the number of design variables. Each of the n columns that contain levels 1, 2,…, m is randomly paired to form a Latin hypercube. This approach, which generates random sample points, ensures that all portions of the design space are represented.

3.3. Surrogate models

In this work, two different surrogate models, i.e., KRG [14] and RBNN [15] models, were tested to find the proper approximation of the objective function.

3.3.1. KRG model

The KRG model [14] is an interpolating meta-modeling technique that employs a trend model, $f(x)$, to capture large-scale variations and a systematic departure, $Z(x)$, to capture small-scale variations. As described by Martin and Simpson [14], Kriging postulation is the combination of a global model and departures of the following form:

$$F(x) = f(x) + Z(x) \tag{5}$$

$F(x)$ represents the surrogate model, and $f(x)$ is the global model which is known function representing the objective function value at the each design points. And, $Z(x)$ represents the localized deviations. $Z(x)$ is the realization of a stochastic process with zero mean and non-zero covariance. A linear polynomial function is used as a trend model and the systematic departure terms follow a Gaussian correlation function. The covariance matrix of $Z(x)$ is given by

$$COV\left[Z\left(x^i\right), Z\left(x^j\right)\right] = \sigma^2 R\left[R\left(x^i, x^j\right)\right], \quad i,j = 1,2,\ldots n_s \tag{6}$$

where R is a correlation matrix with the elements $R(x^i, x^j)$, which is a spatial correlation function (SCF). σ^2 is the process variance representing the scalar of the spatial correlation function quantifying the correlation between any two n_s sampled data points, x^i and x^j. It controls the smoothness of the Kriging model, the effect of nearby points, and differentiability of the surface. The Gaussian function used in this work is the most preferable SCF when used with a gradient based optimization algorithm as it provides a relatively smooth and infinitely differentiable surface.

3.3.2. RBNN model

RBNN model [15] is a two layer network that consists of a hidden layer of radial basis function and a linear output layer. As described by Orr [15], the hidden layer consists of a set of radial basis functions that acts as activation functions, the response of which varies with the distance between the input and the center. The distance between two points is determined by the difference of their coordinates and by a set of parameters. The main advantage of using the radial basis approach is the ability to reduce the computational cost due to the linear nature of the radial basis functions.

$$a = radbas(\|w - p\|b) \tag{7}$$

here, the net input to the *radbas* transfer function is the vector distance between its weight vector w and the input vector p,

Table 2
Boundary conditions and physical properties.

Boundary conditions/physical property	Condition
Mass flow rate at inlet of the calculation domain	0.008826 kg/s
Pressure at outlet of the calculation domain	0 Pa
Top and bottom surfaces of inlet part	Periodic condition
Reference pressure	8.339 MPa
Reference temperature	110 °C
Working fluid	Supercritical CO_2

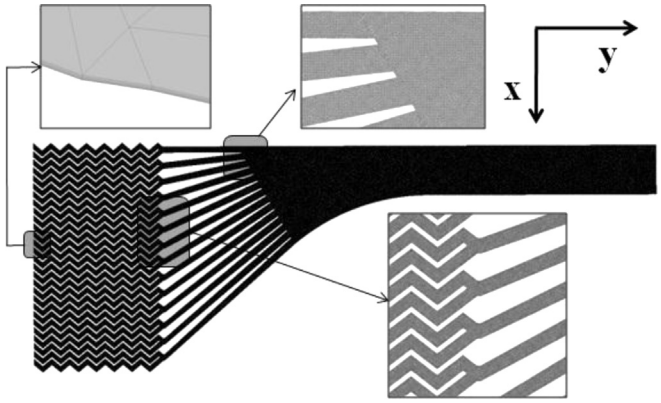

Fig. 3. Example of grid system in the calculation domain of the PCHE.

multiplied by the bias *b*. The transfer function for a radial basis neuron is:

$$radbas(n) = e^{-n^2} \tag{8}$$

The radial basis function has a maximum of 1 when its input is 0. As the distance between *w* and *p* decreases, the output increases. Thus, a radial basis neuron acts as a detector that produces 1 wherever the input *p* is identical to its weight vector *p*. The bias *b* allows the sensitivity of the *radbas* neuron to be adjusted. The parameters for fitting this surrogate model are the spread constant (SC) and a user-defined error goal (EG). The SC value is selected in such a way that should not be so large that each neuron will not respond same for the all input, and that should not be so small that the network will be very high sensitive for every input within design space. And EG is a very small value that will produce over training of the network while a large EG will influence the accuracy of the model. The allowable error goal is decided from the allowable error from the mean input responses. In MATLAB [20], *newrb* is the function for RBNN design.

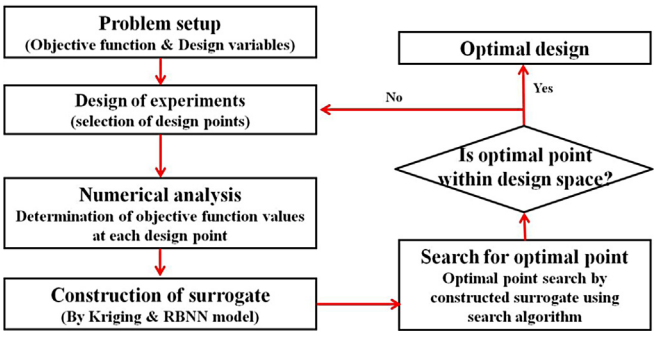

Fig. 4. Flow chart of the optimization procedure.

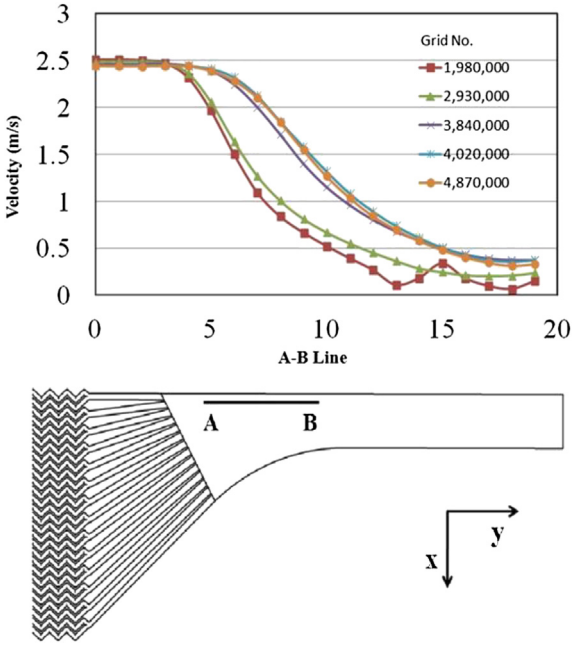

Fig. 5. The results of grid dependency test [13].

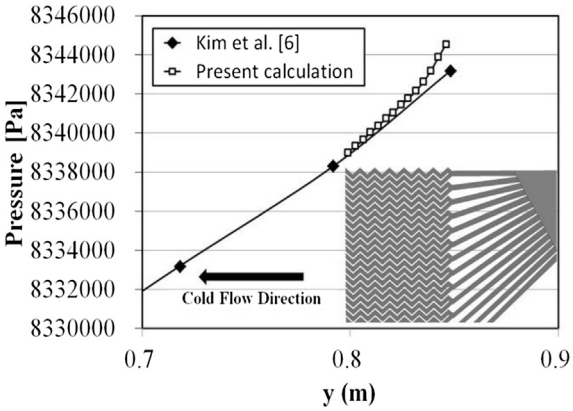

Fig. 6. Validation of numerical results [13].

4. Results and discussion

The numerical model used in this work was constructed through grid dependency test and validation. The grid dependency test was performed to determine the optimum number and the structure of grids in the previous work [13]. As shown in Fig. 5, the test was performed for the velocity profile on the A–B line which is located in the most sensitive region in the aspect of the flow structure [13]. Five different grid systems with the number of grids ranging from about 2.00×10^6 to 4.90×10^6 were tested. The optimum number of grids for the domain was determined as 4,020,000.

Table 3
The design variables and design space.

Variables	Lower	Upper
α	25	75
R/L	0.87	2.62
D/D^0	1.22	1.61

Table 4
Objective function values at twenty six design points selected by LHS.

	α	R/L	D/D^0	F_f	F_P
CASE1	34.769	2.013	1.476	0.05910	1560.26
CASE2	28.192	1.879	1.297	0.07322	1522.51
CASE3	38.423	1.543	1.387	0.06293	1583.49
CASE4	26.731	1.946	1.521	0.06619	1488.95
CASE5	43.538	1.208	1.611	0.05207	1614.92
CASE6	36.962	1.074	1.462	0.05975	1565.89
CASE7	42.808	2.080	1.222	0.06969	1660.97
CASE8	32.577	2.214	1.551	0.05999	1541.36
CASE9	36.231	2.147	1.402	0.06467	1571.75
CASE10	39.154	1.812	1.282	0.06880	1614.56
CASE11	26.000	2.281	1.342	0.06962	1501.04
CASE12	31.846	2.415	1.237	0.07311	1574.43
CASE13	39.885	1.006	1.312	0.06705	1592.26
CASE14	34.038	1.610	1.566	0.05669	1553.92
CASE15	30.385	1.275	1.432	0.06543	1514.27
CASE16	27.462	2.617	1.267	0.07287	1528.13
CASE17	40.615	2.550	1.536	0.05443	1623.38
CASE18	31.115	1.141	1.252	0.07247	1556.04
CASE19	37.692	1.476	1.581	0.05337	1586.43
CASE20	33.308	1.677	1.447	0.06355	1540.73
CASE21	35.500	0.872	1.372	0.06523	1558.19
CASE22	42.077	1.409	1.506	0.05799	1598.15
CASE23	29.654	2.348	1.327	0.06970	1531.39
CASE24	45.000	2.482	1.491	0.05354	1657.45
CASE25	44.269	0.939	1.417	0.05916	1601.90
CASE26	28.923	1.744	1.596	0.05704	1703.69

The results of validation of numerical results were performed compared to the data obtained by Kim et al. [6] in the previous work [13] as shown in Fig. 6. The horizontal and vertical axes represent the location of the measurement point on y-axis and the pressure inside the zigzag channels, respectively. As shown in Fig. 6, the numerical results show reasonable agreements with the reference data, but deviate slightly in the range, $y = 0.839–0.851$ m, as the flow approaches the interface connecting the zigzag channels to the inlet pipes.

The design space was set as shown Table 3. A parametric study was performed in wide ranges of design variables in previous work [13], and then final design ranges were decided. And, twenty six design points were determined by LHS in this design space. Table 4 represents the objective function values calculated at these design points by RANS analysis. These objective function values were used to construct the surrogate model of the objective function.

Table 5 represents the surrogate predictions of the design variables and the objective function for the optimal geometry when the weighting factor β is 4.0×10^{-5}, and corresponding results of RANS calculation. Through the optimizations using RBNN and KRG models, the objective functions were reduced by 1.36% and 1.18%, respectively, compared to that of the reference design. Although the values of the objective function were not much different from that of the reference design, the values of each objective were considerably different from that of the reference design. For example, in the case of the optimum design by KRG, F_f was increased by 7.5% while F_P was decreased by 7.6% in comparison with the reference design. This indicates that only the pressure loss performance was improved. Thus, this optimum design is the pressure loss-oriented design. The orientation of the design can be determined depending on the value of the weighting factor. If the designer chooses a lower value of the weighting factor, the design can be changed to a flow uniformity-oriented design. The errors

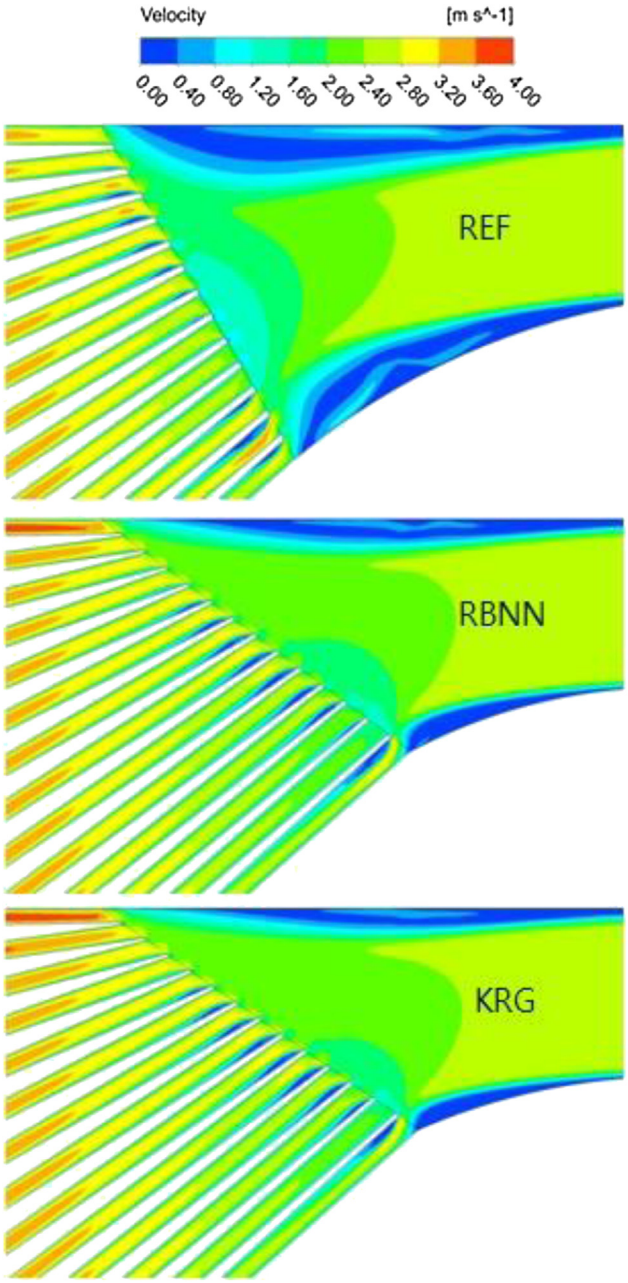

Fig. 7. Velocity field in the inlet part of PCHE.

Table 5
Optimal design predicted by each surrogate model with $\beta = 0.00004$ compared with corresponding RANS results.

	Design variables			Objectives		Objective function, F		
	α	R/L	D/D^0	F_f	F_P	Predict	RANS	Error
Opt. (KRG)	35.0	1.64	1.61	0.0556	1567	0.1148	0.1182	3.01%
Opt. (RBNN)	37.1	1.41	1.61	0.0549	1579	0.1147	0.1180	2.90%
Reference	60.0	1.85	1.80	0.0517	1695	–	0.1196	–

Table 6
Non-dimensional pressure drop in each part.

Section	Non-dimensional pressure drop		
	Reference	KRG	RBNN
Inlet plenum	24.825	16.683	20.665
Inlet pipes	323.40	329.93	322.90
Zigzag channels	1347.2	1219.9	1235.2

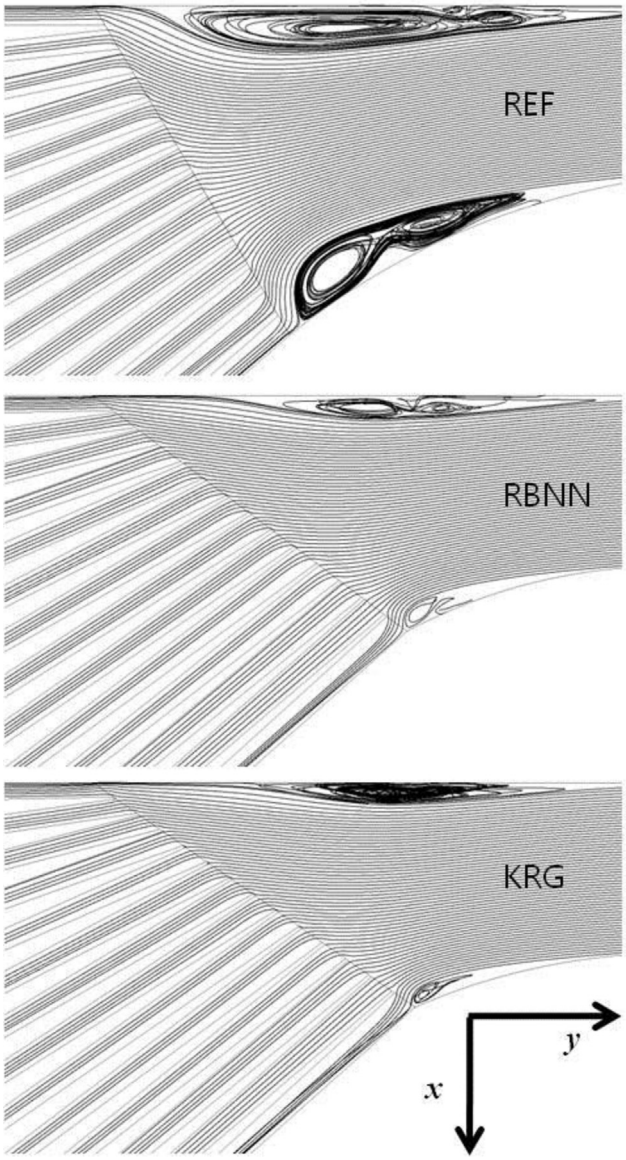

Fig. 8. Streamlines in the inlet part of PCHE.

between the values of the objective function predicted by RBNN and KRG models and calculated by RANS analyses at the optimum points were only 3.01% and 2.90%, respectively.

The velocity and streamline distributions on x–y plane at $z = -0.00005$ m are shown in Figs. 7 and 8, respectively. It can be seen that the extents of the separation zones near the side walls of the inlet plenum were reduced largely by the optimizations. This is directly related to the improvements in the pressure loss performance (F_P) of the optimum designs.

Table 6 shows the non-dimensional pressure drop through each sub-part of the inlet part of PCHE. This non-dimensional pressure drop was defined by replacing the numerator in Eq. (3) by the pressure drop through each sub-part. The pressure drops in the optimum designs were reduced compared to that in the reference design in the inlet plenum as the area of separation zone reduced by the optimization. However, the optimum designs did not affect greatly the pressure drop in the inlet pipes. In the zigzag channels, decreased pressure drops were obtained by the optimizations compared to the reference design, although the decreases in the pressure drop were not as large as those in the inlet plenum.

Fig. 9 represents distribution of the mass flow rate through the inlet pipes. As shown in this figure, the optimum designs show higher flow rates in the channels 1–4, but lower flow rates in remaining channels than the reference design. Therefore, the optimal designs show rather non-uniform distribution of the flow rate compared to the reference design. Thus, the improvement in the pressure drop was obtained at the expense of increased non-uniformity of the flow distribution.

5. Conclusions

In this work, optimization of the inlet part of a PCHE has been performed using 3-D RANS analysis and surrogate modeling. Both RBNN and KRG were employed as surrogate model for the optimization. The objective function was defined as a weighted-sum of two objectives related to uniformity of the mass flow rate distribution and pressure loss, respectively. Through the optimizations using RBNN and KRG models with the weighting factor of 4.0×10^{-5}, the objective functions were reduced by 1.36% and 1.18%, respectively, compared to that of the reference design. In the case of the optimum design by KRG, F_f was increased by 7.5% while F_P was decreased by 7.6% in comparison with the reference design, which indicates that only the pressure loss performance was improved. This result reflects the pressure loss-oriented design. However, the orientation of the design can be changed if a reduced value of the weighting factor is selected. The most of the reduction in the pressure drop was found to occur in the inlet plenum by reducing

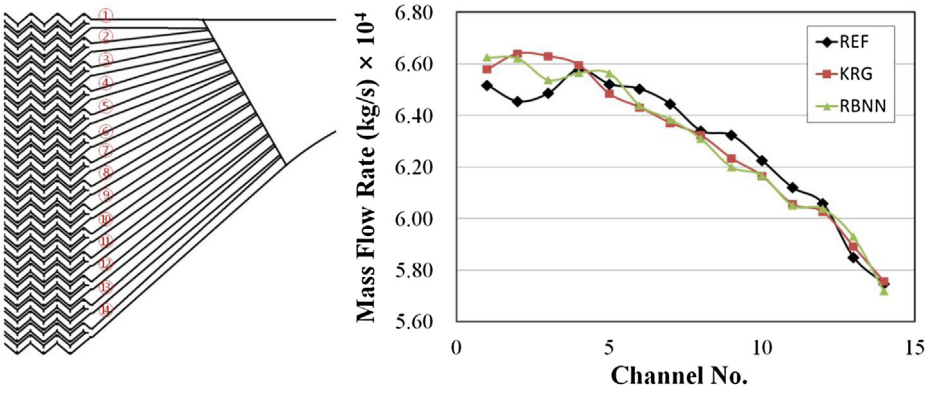

Fig. 9. Distribution of mass flow rates through the inlet pipes.

the separation regions near the side walls. The errors between the values of the objective function predicted by RBNN and KRG models and calculated by RANS analyses at the optimum points were only 3.01% and 2.90%, respectively.

Acknowledgements

This work was supported by the National Research Foundation of Korea (NRF) grant funded by the Korean government (MSIP) through the Multi-phenomena CFD Engineering Research Center (No. 2009-0083510).

References

[1] S.J. Dewson, C. Grady, in: HEATRIC Workshop at MIT, 2003. Cambridge, MA, U.S.A.
[2] D. Southall, R. LePierres, S.J. Dewson, Design considerations for compact heat exchangers, in: Proceedings of ICAPP '08, Anaheim, CA, USA, 2008. Paper No. 8009.
[3] T. Ishizuka, Y. Kato, Y. Muto, K. Nikitin, N.L. Tri, H. Hashimoto, Thermal–hydraulic characteristics of a printed circuit heat exchanger in a supercritical CO_2 loop, in: The 11th International Topical Meeting on Nuclear Reactor Thermal–hydraulics, Avignon, France, 2005. Paper 218.
[4] L. Ngo, Y. Kato, K. Nikitin, N. Tsuzuki, New printed circuit heat exchanger with S-shaped fins for hot water supplier, Exp. Therm. Fluid Sci. 30 (8) (2006) 811–819.
[5] K. Nikitin, Y. Kato, L. Ngo, Printed circuit heat exchanger thermal–hydraulic performance in supercritical CO_2 loop, Int. J. Refrig. 29 (2006) 807–814.
[6] D.E. Kim, M.H. Kim, J.E. Cha, S.O. Kim, Numerical Investigation on thermal–hydraulic performance of new printed circuit heat exchanger model, Nucl. Eng. Des. 238 (2008) 3269–3276.
[7] I.H. Kim, H.C. No, J.I. Lee, B.G. Jeon, Thermal hydraulic performance analysis of the printed circuit heat exchanger using a helium test facility and CFD simulations, Nucl. Eng. Des. 239 (2009) 2399–2408.
[8] S.M. Lee, K.Y. Kim, S.W. Kim, Multi-objective optimization of a double-faced type printed circuit heat exchanger, Appl. Therm. Eng. 60 (2013) 44–50.
[9] J.H. Kim, K.Y. Kim, Optimization of vane diffuser in a mixed-flow pump for high efficiency design, Int. J. Fluid Mach. Syst. 4 (1) (2011) 172–178.
[10] H.M. Kim, K.Y. Kim, Design optimization of rib-roughened channel to enhance turbulent heat transfer, Int. J. Heat Mass Transf. 47 (23) (2004) 5159–5168.
[11] A. Husain, K.Y. Kim, Shape optimization of micro-channel heat sink for micro-electronic cooling, IEEE Trans. Compon. Packag. Technol. 31 (2) (2008) 322–330.
[12] W. Raza, K.Y. Kim, Shape optimization of wire-wrapped fuel assembly using Kriging metamodeling technique, Nucl. Eng. Des. 238 (6) (2008) 1332–1341.
[13] S.M. Lee, G.W. Koo, K.Y. Kim, Parametric study on hydraulic performance of an inlet plenum in a printed-circuit heat exchanger, Sci. China Technol. Sci. 56 (9) (2013) 2137–2142.
[14] J.D. Martin, T.W. Simpson, Use of Kriging models to approximate deterministic computer models, AIAA J. 4 (2005) 853–863.
[15] M.J.L. Orr, Introduction to Radial Basis Neural Networks, Center for Cognitive Science, Edinburgh University, Scotland, UK, 2008. Available at: http://anc.ed.ac.uk/rbf/.
[16] M.D. Mckay, R.J. Beckman, W.J. Conover, A comparison of three methods for selecting values of input variables in the analysis of output from a computer code, Technometrics 21 (1979) 239–245.
[17] CFX-11.0 Solver Theory, Ansys inc, 2008.
[18] F.R. Menter, Two-equation eddy-viscosity turbulence models for engineering applications, AIAA J. 32 (1994) 1598–1605.
[19] J.E. Bardina, P.G. Huang, T. Coakley, Turbulence modeling validation, in: 28th AIAA Fluid Dynamics Conference, Snow Village, CO, U.S.A, 1997. AIAA paper 1997–2121.
[20] MATLAB®, The Language of Technical Computing, Release 14, The Math Works Inc., 2004.